



Range-separated time-dependent density-functional theory with a frequency-dependent second-order Bethe-Salpeter correlation kernel

Elisa Rebolini, Julien Toulouse

► To cite this version:

Elisa Rebolini, Julien Toulouse. Range-separated time-dependent density-functional theory with a frequency-dependent second-order Bethe-Salpeter correlation kernel. 2015. hal-01184145v2

HAL Id: hal-01184145

<https://hal.sorbonne-universite.fr/hal-01184145v2>

Preprint submitted on 13 Oct 2015 (v2), last revised 15 Feb 2016 (v3)

HAL is a multi-disciplinary open access archive for the deposit and dissemination of scientific research documents, whether they are published or not. The documents may come from teaching and research institutions in France or abroad, or from public or private research centers.

L'archive ouverte pluridisciplinaire **HAL**, est destinée au dépôt et à la diffusion de documents scientifiques de niveau recherche, publiés ou non, émanant des établissements d'enseignement et de recherche français ou étrangers, des laboratoires publics ou privés.

Range-separated time-dependent density-functional theory with a frequency-dependent second-order Bethe-Salpeter correlation kernel

Elisa Rebolini^{1,2*†} and Julien Toulouse^{1,2‡}

¹*Sorbonne Universités, UPMC Univ Paris 06, UMR 7616,
Laboratoire de Chimie Théorique, F-75005 Paris, France*

²*CNRS, UMR 7616, Laboratoire de Chimie Théorique, F-75005 Paris, France*

(Dated: October 13, 2015)

We present a range-separated linear-response time-dependent density-functional theory (TDDFT) which combines a density-functional approximation for the short-range response kernel and a frequency-dependent second-order Bethe-Salpeter approximation for the long-range response kernel. This approach goes beyond the adiabatic approximation usually used in linear-response TDDFT and aims at improving the accuracy of calculations of electronic excitation energies of molecular systems. A detailed derivation of the frequency-dependent second-order Bethe-Salpeter correlation kernel is given using many-body Green-function theory. Preliminary tests of this range-separated TDDFT method are presented for the calculation of excitation energies of the Be atom and four small molecules (N₂, CO₂, H₂CO, and C₂H₄). The results suggest that the addition of the long-range second-order Bethe-Salpeter correlation kernel overall slightly improves the excitation energies.

I. INTRODUCTION

Linear-response time-dependent density-functional theory (TDDFT) [1, 2] is nowadays one of the most popular approaches for calculating excitation energies and other response properties of electronic systems. Within the usual adiabatic semilocal density-functional approximations (DFAs), linear-response TDDFT usually provides reasonably accurate low-lying valence electronic excitation energies of molecular systems at a low computational cost. However, these usual adiabatic semilocal DFAs have serious failures. In particular, they give largely underestimated Rydberg [3] and charge-transfer [4] excitation energies and they do not account for double (or multiple) excitations [5].

The problem with Rydberg and charge-transfer excitation energies is alleviated with the use of hybrid approximations in linear-response TDDFT [6], which combine a Hartree-Fock (HF) exchange response kernel with a DFA exchange-correlation response kernel. This problem is essentially solved with range-separated hybrid approximations [7–10], introducing a long-range HF exchange kernel. Research in linear-response TDDFT now aims at an increasingly higher accuracy and reliability, and in particular the inclusion of the effects of the double excitations. Examples of recent developments are: the dressed TDDFT approach (combining TDDFT and the polarization-propagator approach) [11–13], double-hybrid TDDFT methods (combining TDDFT and configuration-interaction singles with doubles correction [CIS(D)]) [14], and range-separated TDDFT ap-

proaches in which the long-range response is treated with density-matrix functional theory (DMFT) [15], multiconfiguration self-consistent-field (MCSCF) theory [16], or the second-order polarization-propagator approximation (SOPPA) [17].

In this work, we explore a range-separated TDDFT approach in which the long-range response is treated with a frequency-dependent second-order Bethe-Salpeter equation (BSE2) correlation kernel. The BSE2 approximation was recently introduced by Zhang *et al.* [18] within the Tamm-Dancoff approximation (TDA) [19]. Building on the work of Sangalli *et al.* [20], we provide an alternative and more general derivation of the BSE2 approximation without using the TDA and we apply it to the range-separated case. We present preliminary tests of this range-separated TDDFT method for the calculation of excitation energies of the Be atom and four small molecules (N₂, CO₂, H₂CO, and C₂H₄).

This paper is organized as follows. In Section II, we summarize the main equations of linear-response TDDFT with range separation. In Section III, we provide a full derivation of the frequency-dependent BSE2 correlation kernel without using the TDA, giving expressions in terms of space-spin coordinates and in a spin-orbital basis. Section IV explains how we practically perform the calculations and gives computational details for the systems tested. The results are given and discussed in Section V. Finally, Section VI contains our conclusions.

II. RANGE-SEPARATED TIME-DEPENDENT DENSITY-FUNCTIONAL THEORY

As a relatively straightforward extension of linear-response TDDFT [1], in range-separated TDDFT [10, 16], the inverse of the frequency-dependent linear-

*Present address: Centre for Theoretical and Computational Chemistry, Department of Chemistry, University of Oslo, P.O. Box 1033 Blindern, N-0315 Oslo, Norway

†Electronic address: elisa.rebolini@kjemi.uio.no

‡Electronic address: julien.toulouse@upmc.fr

response function is expressed as

$$\chi^{-1}(\mathbf{x}_1, \mathbf{x}_2; \mathbf{x}'_1, \mathbf{x}'_2; \omega) = (\chi^{\text{lr}})^{-1}(\mathbf{x}_1, \mathbf{x}_2; \mathbf{x}'_1, \mathbf{x}'_2; \omega) - f_{\text{Hxc}}^{\text{sr}}(\mathbf{x}_1, \mathbf{x}_2; \mathbf{x}'_1, \mathbf{x}'_2; \omega), \quad (1)$$

where $\mathbf{x} = (\mathbf{r}, \sigma)$ stands for space-spin coordinates. In this expression, $\chi^{\text{lr}}(\mathbf{x}_1, \mathbf{x}_2; \mathbf{x}'_1, \mathbf{x}'_2; \omega)$ is the linear-response function associated with the long-range (lr) interacting Hamiltonian

$$\hat{H}^{\text{lr}} = \hat{T} + \hat{V}_{\text{ne}} + \hat{W}_{\text{ee}}^{\text{lr}} + \hat{V}_{\text{Hxc}}^{\text{sr}}, \quad (2)$$

where \hat{T} is the kinetic-energy operator, \hat{V}_{ne} is the nuclei-electron interaction operator, $\hat{W}_{\text{ee}}^{\text{lr}}$ is a long-range electron-electron interaction operator, and $\hat{V}_{\text{Hxc}}^{\text{sr}}$ is a corresponding short-range (sr) Hartree-exchange-correlation (Hxc) potential operator. Additionally, $f_{\text{Hxc}}^{\text{sr}}(\mathbf{x}_1, \mathbf{x}_2; \mathbf{x}'_1, \mathbf{x}'_2; \omega) = f_{\text{Hxc}}^{\text{sr}}(\mathbf{x}_1, \mathbf{x}_2; \omega) \delta(\mathbf{x}_1, \mathbf{x}'_1) \delta(\mathbf{x}_2, \mathbf{x}'_2)$ is the short-range Hxc kernel related to the functional derivative of the short-range Hxc potential with respect to the density (and δ is the delta function). In practice, the long-range electron-electron interaction is defined with the error function as $w_{\text{ee}}^{\text{lr}}(\mathbf{r}_1, \mathbf{r}_2) = \text{erf}(\mu|\mathbf{r}_1 - \mathbf{r}_2|)/|\mathbf{r}_1 - \mathbf{r}_2|$, where the parameter μ controls the range of the interaction. Even though Eq. (1) is written with functions depending on four space-spin coordinates for generality, range-separated TDDFT only gives exactly the diagonal part of the linear-response function $\chi(\mathbf{x}_1, \mathbf{x}_2; \omega) = \chi(\mathbf{x}_1, \mathbf{x}_2; \mathbf{x}_1, \mathbf{x}_2; \omega)$, as usual TDDFT.

In the time-dependent range-separated hybrid (TDRSH) scheme [10], the long-range linear-response function $\chi^{\text{lr}}(\omega)$ is calculated at the HF level. More precisely, the inverse of the long-range linear-response function is approximated as

$$(\chi^{\text{lr}})^{-1}(\mathbf{x}_1, \mathbf{x}_2; \mathbf{x}'_1, \mathbf{x}'_2; \omega) \approx (\chi_0)^{-1}(\mathbf{x}_1, \mathbf{x}_2; \mathbf{x}'_1, \mathbf{x}'_2; \omega) - f_{\text{Hxc}, \text{HF}}^{\text{lr}}(\mathbf{x}_1, \mathbf{x}_2; \mathbf{x}'_1, \mathbf{x}'_2), \quad (3)$$

where $\chi_0(\omega)$ is the non-interacting linear-response function associated with the range-separated-hybrid (RSH) reference Hamiltonian [21]

$$\hat{H}_0 = \hat{T} + \hat{V}_{\text{ne}} + \hat{V}_{\text{Hxc}, \text{HF}}^{\text{lr}} + \hat{V}_{\text{Hxc}}^{\text{sr}}, \quad (4)$$

with the long-range HF potential operator $\hat{V}_{\text{Hxc}, \text{HF}}^{\text{lr}}$, and $f_{\text{Hxc}}^{\text{lr}}(\mathbf{x}_1, \mathbf{x}_2; \mathbf{x}'_1, \mathbf{x}'_2)$ is the corresponding long-range HF kernel. The latter is the sum of a long-range Hartree kernel,

$$f_{\text{H}}^{\text{lr}}(\mathbf{x}_1, \mathbf{x}_2; \mathbf{x}'_1, \mathbf{x}'_2) = w_{\text{ee}}^{\text{lr}}(\mathbf{r}_1, \mathbf{r}_2) \delta(\mathbf{x}_1, \mathbf{x}'_1) \delta(\mathbf{x}_2, \mathbf{x}'_2), \quad (5)$$

and a long-range HF exchange kernel,

$$f_{\text{x}, \text{HF}}^{\text{lr}}(\mathbf{x}_1, \mathbf{x}_2; \mathbf{x}'_1, \mathbf{x}'_2) = -w_{\text{ee}}^{\text{lr}}(\mathbf{r}_1, \mathbf{r}_2) \delta(\mathbf{x}_1, \mathbf{x}'_2) \delta(\mathbf{x}_2, \mathbf{x}'_1). \quad (6)$$

To go beyond the HF level, it was proposed to calculate $\chi^{\text{lr}}(\omega)$ at the linear-response MCSCF level [16] or at the SOPPA level [17]. In the present work, we

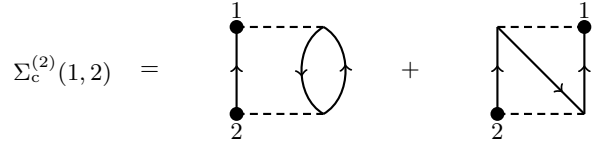


Figure 1: Feynman diagrams of the second-order correlation self-energy $\Sigma_c^{(2)}(1, 2)$. The time axis is vertical. The dots represent the outer variables 1 and 2. Horizontal dashed lines represent electron-electron interactions w_{ee} . Arrowed lines represent one-particle Green functions G . The first diagram is the direct contribution of Eq. (9) and the second diagram is the exchange contribution of Eq. (10).

explore the recently proposed BSE2 approximation [18]. We thus propose to approximate the inverse of the long-range linear-response function as

$$(\chi^{\text{lr}})^{-1}(\mathbf{x}_1, \mathbf{x}_2; \mathbf{x}'_1, \mathbf{x}'_2; \omega) \approx (\chi_0)^{-1}(\mathbf{x}_1, \mathbf{x}_2; \mathbf{x}'_1, \mathbf{x}'_2; \omega) - f_{\text{Hxc}, \text{HF}}^{\text{lr}}(\mathbf{x}_1, \mathbf{x}_2; \mathbf{x}'_1, \mathbf{x}'_2) - f_{\text{c}, \text{BSE2}}^{\text{lr}}(\mathbf{x}_1, \mathbf{x}_2; \mathbf{x}'_1, \mathbf{x}'_2; \omega), \quad (7)$$

with the long-range BSE2 frequency-dependent correlation kernel $f_{\text{c}, \text{BSE2}}^{\text{lr}}(\omega)$ for which we offer an alternative and more general derivation compared to Ref. 18.

III. SECOND-ORDER BETHE-SALPETER CORRELATION KERNEL

In this Section, we provide a derivation of the BSE2 correlation kernel. For more details, see Ref. 22. We consider an arbitrary electron-electron interaction w_{ee} in the derivation instead of the long-range one.

A. Second-order correlation self-energy

The starting point is the second-order correlation self-energy as a functional of the one-electron Green function $G(1, 2)$ where $1 = (\mathbf{x}_1, t_1)$ and $2 = (\mathbf{x}_2, t_2)$ stand for space-spin-time coordinates (see, e.g., Ref. 23)

$$\Sigma_c^{(2)}(1, 2) = i \int d3d3'd4d4'd5d5' G(3, 3') \bar{w}_{\text{ee}}(3', 4; 2, 4') \chi_{\text{IP}}(4', 5; 4, 5') w_{\text{ee}}(5', 1; 5, 3), \quad (8)$$

where $w_{\text{ee}}(1, 2; 1', 2') = w_{\text{ee}}(1, 2) \delta(1, 1') \delta(2, 2')$ is an arbitrary electron-electron interaction, $\bar{w}_{\text{ee}}(1, 2; 1', 2') = w_{\text{ee}}(1, 2; 1', 2') - w_{\text{ee}}(2, 1; 1', 2')$ is the corresponding antisymmetrized interaction, and $\chi_{\text{IP}}(1, 2; 1', 2') = -iG(1, 2')G(2, 1')$ is the independent-particle (IP) four-point linear-response function. The presence of the antisymmetrized interaction \bar{w}_{ee} in Eq. (8) means that the second-order correlation self-energy can be decomposed as $\Sigma_c^{(2)} = \Sigma_c^{(2\text{d})} + \Sigma_c^{(2\text{x})}$ with a direct contribution

$$\Sigma_c^{(2\text{d})}(1, 2) = i G(1, 2) \int d3d4 w_{\text{ee}}(2, 3) \times \chi_{\text{IP}}(3, 4; 3, 4) w_{\text{ee}}(4, 1), \quad (9)$$

and an exchange contribution

$$\begin{aligned} \Sigma_c^{(2x)}(1, 2) = & -i \int d3d4 G(1, 3)w_{ee}(2, 3) \\ & \times \chi_{IP}(3, 4; 2, 4)w_{ee}(4, 1). \end{aligned} \quad (10)$$

The Feynman diagrams of these terms are represented in Figure 1.

B. Second-order Bethe-Salpeter correlation kernel in the time domain

The second-order Bethe-Salpeter correlation kernel is defined as the functional derivative of the second-order correlation self-energy with respect to the Green function

$$\Xi_c^{(2)}(1, 4; 2, 3) = i \frac{\delta \Sigma_c^{(2)}(1, 2)}{\delta G(3, 4)}. \quad (11)$$

Taking the derivative of Eq. (8) generates three terms

$$\begin{aligned} \Xi_c^{(2)}(1, 4; 2, 3) = & \\ & - \int d5d5'd6d6' \bar{w}_{ee}(4, 5; 2, 5') \chi_{IP}(5', 6; 5, 6') w_{ee}(6', 1; 6, 3) \\ & - \int d5d5'd6d6' \bar{w}_{ee}(5, 4; 2, 6) \chi_{IP}(5', 6; 6', 5) w_{ee}(6', 1; 3, 5') \\ & - \int d5d5'd6d6' \bar{w}_{ee}(5, 6; 2, 3) \chi_{IP}(6', 5'; 6, 5) w_{ee}(4, 1; 5', 6'), \end{aligned}$$

which, as done for the correlation self-energy, can be decomposed as $\Xi_c^{(2)} = \Xi_c^{(2d)} + \Xi_c^{(2x)}$, with a direct contribution

$$\begin{aligned} \Xi_c^{(2d)}(1, 4; 2, 3) = & \\ & - \delta(1, 3) \delta(2, 4) \int d5d6 w_{ee}(2, 5) \chi_{IP}(5, 6; 5, 6) w_{ee}(6, 1) \\ & - w_{ee}(2, 4) \chi_{IP}(1, 4; 3, 2) w_{ee}(3, 1) \\ & - w_{ee}(2, 3) \chi_{IP}(1, 4; 3, 2) w_{ee}(4, 1), \end{aligned} \quad (13)$$

and an exchange contribution

$$\begin{aligned} \Xi_c^{(2x)}(1, 4; 2, 3) = & \\ & \delta(1, 3) \int d5 w_{ee}(2, 4) \chi_{IP}(4, 5; 2, 5) w_{ee}(5, 1) \\ & + \delta(2, 4) \int d5 w_{ee}(2, 5) \chi_{IP}(1, 5; 3, 5) w_{ee}(3, 1) \\ & + w_{ee}(2, 3) \chi_{IP}(1, 4; 2, 3) w_{ee}(4, 1). \end{aligned} \quad (14)$$

The Feynman diagrams of these six terms are represented in Figure 2. Similar kernel diagrams are shown in Ref. 24.

Introducing explicitly the time variables, using an instantaneous spin-independent electron-electron interaction $w_{ee}(1, 2) = w_{ee}(\mathbf{r}_1, \mathbf{r}_2) \delta(t_1, t_2)$ and time-translation invariance, we found that the second-order Bethe-Salpeter correlation kernel is composed of a

particle-hole/hole-particle (ph/hp) part and a particle-particle/hole-hole (pp/hh) part, which non-trivially depend on only one time difference $t_1 - t_2$,

$$\begin{aligned} \Xi_c^{(2)}(\mathbf{x}_1 t_1, \mathbf{x}_4 t_4; \mathbf{x}_2 t_2, \mathbf{x}_3 t_3) = & \\ = & \delta(t_1, t_3) \delta(t_2, t_4) \Xi_c^{(2, \text{ph/hp})}(\mathbf{x}_1, \mathbf{x}_4; \mathbf{x}_2, \mathbf{x}_3; t_1 - t_2) \\ & + \delta(t_1, t_4) \delta(t_2, t_3) \Xi_c^{(2, \text{pp/hh})}(\mathbf{x}_1, \mathbf{x}_4; \mathbf{x}_2, \mathbf{x}_3; t_1 - t_2), \end{aligned} \quad (15)$$

with the ph/hp kernel

$$\begin{aligned} \Xi_c^{(2, \text{ph/hp})}(\mathbf{x}_1, \mathbf{x}_4; \mathbf{x}_2, \mathbf{x}_3; \tau) = & \\ = & - \delta(\mathbf{x}_1, \mathbf{x}_3) \delta(\mathbf{x}_2, \mathbf{x}_4) \int d\mathbf{x}_5 d\mathbf{x}_6 w_{ee}(\mathbf{r}_2, \mathbf{r}_5) \\ & \times \chi_{IP}(\mathbf{x}_5, \mathbf{x}_6; \mathbf{x}_5, \mathbf{x}_6; -\tau) w_{ee}(\mathbf{r}_6, \mathbf{r}_1) \\ & - w_{ee}(\mathbf{r}_2, \mathbf{r}_4) \chi_{IP}(\mathbf{x}_1, \mathbf{x}_4; \mathbf{x}_3, \mathbf{x}_2; \tau) w_{ee}(\mathbf{r}_3, \mathbf{r}_1) \\ & + \delta(\mathbf{x}_1, \mathbf{x}_3) \int d\mathbf{x}_5 w_{ee}(\mathbf{r}_2, \mathbf{r}_4) \\ & \times \chi_{IP}(\mathbf{x}_4, \mathbf{x}_5; \mathbf{x}_2, \mathbf{x}_5; -\tau) w_{ee}(\mathbf{r}_5, \mathbf{r}_1) \\ & + \delta(\mathbf{x}_2, \mathbf{x}_4) \int d\mathbf{x}_5 w_{ee}(\mathbf{r}_2, \mathbf{r}_5) \\ & \times \chi_{IP}(\mathbf{x}_1, \mathbf{x}_5; \mathbf{x}_3, \mathbf{x}_5; \tau) w_{ee}(\mathbf{r}_3, \mathbf{r}_1), \end{aligned} \quad (16)$$

and the pp/hh kernel

$$\begin{aligned} \Xi_c^{(2, \text{pp/hh})}(\mathbf{x}_1, \mathbf{x}_4; \mathbf{x}_2, \mathbf{x}_3; \tau) = & \\ = & - w_{ee}(\mathbf{r}_2, \mathbf{r}_3) \chi_{IP}^{\text{pp/hh}}(\mathbf{x}_1, \mathbf{x}_4; \mathbf{x}_3, \mathbf{x}_2; \tau) w_{ee}(\mathbf{r}_4, \mathbf{r}_1) \\ & + w_{ee}(\mathbf{r}_2, \mathbf{r}_3) \chi_{IP}^{\text{pp/hh}}(\mathbf{x}_1, \mathbf{x}_4; \mathbf{x}_2, \mathbf{x}_3; \tau) w_{ee}(\mathbf{r}_4, \mathbf{r}_1), \end{aligned} \quad (17)$$

where $\chi_{IP}(\mathbf{x}_1, \mathbf{x}_2; \mathbf{x}'_1, \mathbf{x}'_2; \tau = t_1 - t_2) = \chi_{IP}(\mathbf{x}_1 t_1, \mathbf{x}_2 t_2; \mathbf{x}'_1 t_1, \mathbf{x}'_2 t_2)$ is the IP (ph/hp) linear-response function and $\chi_{IP}^{\text{pp/hh}}(\mathbf{x}_1, \mathbf{x}_2; \mathbf{x}'_1, \mathbf{x}'_2; \tau = t_1 - t_2) = \chi_{IP}(\mathbf{x}_1 t_1, \mathbf{x}_2 t_1; \mathbf{x}'_1 t_2, \mathbf{x}'_2 t_2)$ is the IP pp/hh linear-response function. As the names suggest, the former describes the independent propagation of one particle and one hole, and the latter describes the independent propagation of either two particles or two holes, depending on the sign of $t_1 - t_2$. Because of the different delta functions on the time variables in Eq. (15), the ph/hp and pp/hh contributions need to be treated separately.

C. Effective second-order Bethe-Salpeter correlation kernel in the frequency domain

The Bethe-Salpeter kernel that we derived must be used in the general Bethe-Salpeter equation in the time domain which is [25, 26]

$$\begin{aligned} \chi(1, 2; 1', 2') = & \chi_{IP}(1, 2; 1', 2') + \int d3d4d5d6 \\ & \chi_{IP}(1, 4; 1', 3) \Xi_{\text{Hxc}}(3, 6; 4, 5) \chi(5, 2; 6, 2'), \end{aligned} \quad (18)$$

where $\chi(1, 2; 1', 2')$ is the interacting four-point linear-response function and Ξ_{Hxc} is the Bethe-Salpeter Hxc

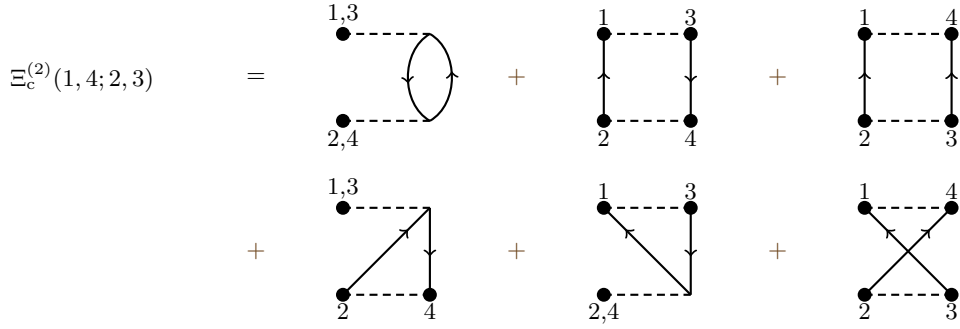


Figure 2: Feynman diagrams of the second-order Bethe-Salpeter correlation kernel $\Xi_c^{(2)}(1, 4; 2, 3)$. The three upper diagrams are the direct contributions of Eq. (13) and the three lower diagrams are the exchange contributions of Eq. (14). The four diagrams on the left correspond to ph/hp terms and the two diagrams on the right correspond to pp/hh diagrams. Since the kernel is the functional derivative of the self-energy with respect to the Green function, these diagrams can be obtained from the ones of Figure 1 by removing one of the arrowed lines.

kernel. Written explicitly with time variables, and setting $t'_1 = t_1^+$ and $t'_2 = t_2^+$ (where $t^+ = t + 0^+$ refers to a time variable with an infinitesimal positive shift) to extract the (ph/hp) linear-response function, the equation becomes

$$\begin{aligned} \chi(\mathbf{x}_1 t_1, \mathbf{x}_2 t_2; \mathbf{x}'_1 t'_1, \mathbf{x}'_2 t'_2) &= \chi_{\text{IP}}(\mathbf{x}_1 t_1, \mathbf{x}_2 t_2; \mathbf{x}'_1 t'_1, \mathbf{x}'_2 t'_2) \\ &+ \int d\mathbf{x}_3 dt_3 d\mathbf{x}_4 dt_4 d\mathbf{x}_5 dt_5 d\mathbf{x}_6 dt_6 \Xi_{\text{Hxc}}(\mathbf{x}_3 t_3, \mathbf{x}_6 t_6; \mathbf{x}_4 t_4, \mathbf{x}_5 t_5) \chi(\mathbf{x}_5 t_5, \mathbf{x}_2 t_2; \mathbf{x}_6 t_6, \mathbf{x}'_2 t'_2), \end{aligned} \quad (19)$$

where $\Xi_{\text{Hxc}}(\mathbf{x}_3 t_3, \mathbf{x}_6 t_6; \mathbf{x}_4 t_4, \mathbf{x}_5 t_5) = f_{\text{Hx, HF}}(\mathbf{x}_3, \mathbf{x}_6; \mathbf{x}_4, \mathbf{x}_5) + \Xi_c^{(2)}(\mathbf{x}_3 t_3, \mathbf{x}_6 t_6; \mathbf{x}_4 t_4, \mathbf{x}_5 t_5)$ is taken as the sum of time-independent HF kernel $f_{\text{Hx, HF}}$ and the second-order correlation kernel $\Xi_c^{(2)}$. Because of the time dependence in $\Xi_c^{(2)}$, in Eq. (19) the time variables t_3 and t_4 cannot be equated, and neither can the time variables t_5 and t_6 . Consequently, Eq. (19) is not a closed equation for the (ph/hp) linear-response function $\chi(\mathbf{x}_1 t_1, \mathbf{x}_2 t_2; \mathbf{x}'_1 t'_1, \mathbf{x}'_2 t'_2)$.

To close the equation, Zhang *et al.* [18] followed Strinati [27] and used an explicit time-dependent form in the TDA for the ph/hp amplitudes [27, 28] with which χ in Eq. (19) can be expressed. Here, instead, following Sangalli *et al.* [20] (see also Ref. 29), we work in Fourier space and define an effective kernel depending on only one frequency without using the TDA. Introducing the decomposition of $\Xi_c^{(2)}$ in ph/hp and pp/hh terms given in Eq. (15) and Fourier transforming Eq. (19) gives

$$\begin{aligned} \chi(\omega) &= \chi_{\text{IP}}(\omega) + \chi_{\text{IP}}(\omega) f_{\text{Hx}} \chi(\omega) \\ &+ \int \frac{d\omega'}{2\pi} \frac{d\omega''}{2\pi} \chi_{\text{IP}}(\omega', \omega) \Xi_c^{(2, \text{ph/hp})}(\omega' - \omega'') \chi(\omega'', \omega) \\ &+ \int \frac{d\omega'}{2\pi} \frac{d\omega''}{2\pi} \chi_{\text{IP}}(\omega', \omega) \Xi_c^{(2, \text{pp/hh})}(\omega' + \omega'') \chi(\omega'', \omega), \end{aligned} \quad (20)$$

where the space-spin variables have been dropped for conciseness (all the quantities depend on four space-spin

variables), and the integrations over ω' and ω'' are from $-\infty$ to $+\infty$. In this expression, $\chi(\omega', \omega)$ is the double Fourier transform

$$\chi(\omega', \omega) = \int d\tau_1 d\tau e^{i\omega' \tau_1} e^{i\omega \tau} \chi(\tau_1, \tau_2 = 0^-, \tau), \quad (21)$$

with the variables $\tau_1 = t_1 - t'_1$, $\tau_2 = t_2 - t'_2$, and $\tau = (t_1 + t'_1)/2 - (t_2 + t'_2)/2$, and similarly for $\chi_{\text{IP}}(\omega', \omega)$. As a special case, $\chi(\omega)$ is just the Fourier transform of the (ph/hp) linear-response function $\chi(\tau_1 = 0, \tau_2 = 0, \tau)$, and similarly for $\chi_{\text{IP}}(\omega)$. Obviously, $\Xi_c^{(2, \text{ph/hp})}(\omega)$ and $\Xi_c^{(2, \text{pp/hh})}(\omega)$ are the Fourier transforms of $\Xi_c^{(2, \text{ph/hp})}(\tau)$ and $\Xi_c^{(2, \text{pp/hh})}(\tau)$ given in Eqs. (16) and (17), respectively. Eq. (20) can be rewritten as an effective Bethe-Salpeter equation involving only one frequency [20]

$$\chi(\omega) = \chi_{\text{IP}}(\omega) + \chi_{\text{IP}}(\omega) f_{\text{Hx}} \chi(\omega) + \chi_{\text{IP}}(\omega) \tilde{\Xi}_c^{(2)}(\omega) \chi(\omega), \quad (22)$$

or, equivalently,

$$\chi^{-1}(\omega) = \chi_{\text{IP}}^{-1}(\omega) - f_{\text{Hx}} - \tilde{\Xi}_c^{(2)}(\omega), \quad (23)$$

with an effective correlation kernel defined as

$$\begin{aligned} \tilde{\Xi}_c^{(2)}(\omega) &= \chi_{\text{IP}}^{-1}(\omega) \int \frac{d\omega'}{2\pi} \frac{d\omega''}{2\pi} \chi_{\text{IP}}(\omega', \omega) \\ &\Xi_c^{(2, \text{ph/hp})}(\omega' - \omega'') \chi(\omega'', \omega) \chi^{-1}(\omega) \\ &+ \chi_{\text{IP}}^{-1}(\omega) \int \frac{d\omega'}{2\pi} \frac{d\omega''}{2\pi} \chi_{\text{IP}}(\omega', \omega) \\ &\Xi_c^{(2, \text{pp/hh})}(\omega' + \omega'') \chi(\omega'', \omega) \chi^{-1}(\omega). \end{aligned} \quad (24)$$

To keep only second-order terms in Eq. (24) we must replace both the IP linear-response function χ_{IP} and interacting linear-response function χ by the non-interacting linear-response function χ_0 , and we finally arrive at the

BSE2 correlation kernel

$$\begin{aligned}
f_{c,\text{BSE2}}(\omega) &= \chi_0^{-1}(\omega) \int \frac{d\omega'}{2\pi} \frac{d\omega''}{2\pi} \chi_0(\omega', \omega) \\
&\quad \Xi_c^{(2,\text{ph/hp})}(\omega' - \omega'') \chi_0(\omega'', \omega) \chi_0^{-1}(\omega) \\
&\quad + \chi_0^{-1}(\omega) \int \frac{d\omega'}{2\pi} \frac{d\omega''}{2\pi} \chi_0(\omega', \omega) \\
&\quad \Xi_c^{(2,\text{pp/hh})}(\omega' + \omega'') \chi_0(\omega'', \omega) \chi_0^{-1}(\omega),
\end{aligned} \tag{25}$$

where $\Xi_c^{(2,\text{ph/hp})}$ and $\Xi_c^{(2,\text{pp/hh})}$ are obtained from Eqs. (16) and (17) with the replacement of χ_{IP} by χ_0 as well.

We note that, in Eq. (23), $\chi_{\text{IP}}^{-1}(\omega)$ could also be expanded to second order, leading to self-energy contributions to the effective kernel [20]. However, in this work, we do not consider such self-energy contributions.

D. Expressions in a spin-orbital basis

We now give expressions in the orthonormal canonical spin-orbital basis $\{\varphi_p\}$ of the reference non-interacting Hamiltonian. Any function $F(\mathbf{x}_1, \mathbf{x}_2; \mathbf{x}'_1, \mathbf{x}'_2)$ depending on four space-spin coordinates can be expanded in the basis of products of two spin orbitals, and its matrix elements are defined as

$$\begin{aligned}
F_{pq,rs} &= \int d\mathbf{x}_1 d\mathbf{x}'_1 d\mathbf{x}_2 d\mathbf{x}'_2 \varphi_p(\mathbf{x}'_1) \varphi_q^*(\mathbf{x}_1) \\
&\quad F(\mathbf{x}_1, \mathbf{x}_2; \mathbf{x}'_1, \mathbf{x}'_2) \varphi_r^*(\mathbf{x}_2) \varphi_s(\mathbf{x}'_2),
\end{aligned} \tag{26}$$

where p, q, r, s refer to any (occupied or virtual) spin orbital. In the following, the indices i, j, k, l will refer to occupied spin orbitals and the indices a, b, c, d to virtual spin orbitals.

Using the expression of the Fourier transform of the non-interacting (ph/ph) linear-response function,

$$\begin{aligned}
\chi_0(\mathbf{x}_1, \mathbf{x}_2; \mathbf{x}'_1, \mathbf{x}'_2; \omega) &= \\
&\sum_{kc} \frac{\varphi_k^*(\mathbf{x}'_1) \varphi_c(\mathbf{x}_1) \varphi_c^*(\mathbf{x}'_2) \varphi_k(\mathbf{x}_2)}{\omega - (\varepsilon_c - \varepsilon_k) + i0^+} \\
&- \sum_{kc} \frac{\varphi_k^*(\mathbf{x}'_2) \varphi_c(\mathbf{x}_2) \varphi_c^*(\mathbf{x}'_1) \varphi_k(\mathbf{x}_1)}{\omega + (\varepsilon_c - \varepsilon_k) - i0^+},
\end{aligned} \tag{27}$$

and of the non-interacting pp/hh linear-response function,

$$\begin{aligned}
\chi_0^{\text{pp/hh}}(\mathbf{x}_1, \mathbf{x}_2; \mathbf{x}'_1, \mathbf{x}'_2; \omega) &= \\
&\sum_{kl} \frac{\varphi_k^*(\mathbf{x}'_1) \varphi_l(\mathbf{x}_1) \varphi_l^*(\mathbf{x}'_2) \varphi_k(\mathbf{x}_2)}{\omega - (\varepsilon_k + \varepsilon_l) - i0^+} \\
&- \sum_{cd} \frac{\varphi_c^*(\mathbf{x}'_1) \varphi_d(\mathbf{x}_1) \varphi_d^*(\mathbf{x}'_2) \varphi_c(\mathbf{x}_2)}{\omega + (\varepsilon_c + \varepsilon_d) + i0^+},
\end{aligned} \tag{28}$$

where ε_p are the spin-orbital energies, we find the matrix elements of the Fourier transform of the ph/hp second-

order correlation kernel,

$$\begin{aligned}
\Xi_{c,pq,rs}^{(2,\text{ph/hp})}(\omega) &= - \sum_{kc} \frac{\langle rc||pk\rangle \langle kq||cs\rangle}{\omega - (\varepsilon_c - \varepsilon_k) + i0^+} \\
&\quad + \sum_{kc} \frac{\langle rk||pc\rangle \langle cq||ks\rangle}{\omega + (\varepsilon_c - \varepsilon_k) - i0^+},
\end{aligned} \tag{29}$$

and of the pp/hh second-order correlation kernel,

$$\begin{aligned}
\Xi_{c,pq,rs}^{(2,\text{pp/hh})}(\omega) &= -\frac{1}{2} \sum_{kl} \frac{\langle qr||kl\rangle \langle lk||sp\rangle}{\omega - (\varepsilon_k + \varepsilon_l) - i0^+} \\
&\quad + \frac{1}{2} \sum_{cd} \frac{\langle qr||cd\rangle \langle dc||sp\rangle}{\omega - (\varepsilon_c + \varepsilon_d) + i0^+}.
\end{aligned} \tag{30}$$

where $\langle pq||rs\rangle = \langle pq|rs\rangle - \langle pq|sr\rangle$ are the antisymmetrized two-electron integrals associated with the interaction w_{ee} .

The matrices of $\chi_0(\omega)$ and $\chi_0(\omega', \omega)$ are both diagonal with elements in the occupied-virtual/occupied-virtual spin-orbital product block given by

$$\chi_{0,ia,ia}(\omega) = \frac{1}{\omega - (\varepsilon_a - \varepsilon_i) + i0^+}, \tag{31}$$

and

$$\begin{aligned}
\chi_{0,ia,ia}(\omega', \omega) &= i\chi_{0,ia,ia}(\omega) e^{i\omega'0^+} \\
&\times \left(\frac{1}{\omega' + \omega/2 - \varepsilon_a + i0^+} - \frac{1}{\omega' - \omega/2 - \varepsilon_i - i0^+} \right),
\end{aligned} \tag{32}$$

and, for the virtual-occupied/virtual-occupied block, $\chi_{0,ai,ai}(\omega', \omega) = \chi_{0,ia,ia}(\omega', -\omega)$ and $\chi_{0,ai,ai}(\omega) = \chi_{0,ia,ia}(-\omega)$. The matrix elements of the BSE2 correlation kernel are then found straightforwardly by doing the matrix multiplications and contour-integrating over the frequencies in the upper-half complex plane in Eq. (25). For the matrix elements in the occupied-virtual/occupied-virtual (ov/ov) block (contributing to the linear-response matrix usually denoted by \mathbf{A}), we find

$$\begin{aligned}
f_{c,\text{BSE2},ia,jb}(\omega) &= - \sum_{kc} \frac{\langle jc||ik\rangle \langle ka||cb\rangle}{\omega - (\varepsilon_b + \varepsilon_c - \varepsilon_i - \varepsilon_k)} \\
&- \sum_{kc} \frac{\langle jk||ic\rangle \langle ca||kb\rangle}{\omega - (\varepsilon_a + \varepsilon_c - \varepsilon_j - \varepsilon_k)} \\
&\quad + \frac{1}{2} \sum_{kl} \frac{\langle aj||kl\rangle \langle lk||bi\rangle}{\omega - (\varepsilon_a + \varepsilon_b - \varepsilon_k - \varepsilon_l)} \\
&\quad + \frac{1}{2} \sum_{cd} \frac{\langle aj||cd\rangle \langle dc||bi\rangle}{\omega - (\varepsilon_c + \varepsilon_d - \varepsilon_i - \varepsilon_j)}.
\end{aligned} \tag{33}$$

Note that the denominators of Eq. (33) contain the sum of two virtual spin-orbital energies minus the sum of two occupied spin-orbital energies, i.e. a non-interacting double-excitation energy. Thus, the denominators are small whenever ω is close to a non-interacting double-excitation energy. The matrix elements in Eq. (33) are

identical (at least for real-valued spin-orbitals) to the kernel matrix elements recently derived by Zhang *et al.* [18] in the TDA [30]. The matrix elements in Eq. (33) also show some similitude with the SOPPA kernel [12, 31–33] and the second RPA kernel [20]. Similarly, for the matrix elements of the BSE2 correlation kernel in the occupied-virtual/virtual-occupied (ov/vv) block (contributing to the linear-response matrix usually denoted by \mathbf{B}), we find

$$\begin{aligned} f_{c,\text{BSE2},ia,bj} = & - \sum_{kc} \frac{\langle bc||ik\rangle\langle ka||cj\rangle}{-(\varepsilon_b + \varepsilon_c - \varepsilon_i - \varepsilon_k)} \\ & - \sum_{kc} \frac{\langle bk||ic\rangle\langle ca||kj\rangle}{-(\varepsilon_a + \varepsilon_c - \varepsilon_j - \varepsilon_k)} \\ & + \frac{1}{2} \sum_{kl} \frac{\langle ab||kl\rangle\langle lk||ji\rangle}{-(\varepsilon_a + \varepsilon_b - \varepsilon_k - \varepsilon_l)} \\ & + \frac{1}{2} \sum_{cd} \frac{\langle ab||cd\rangle\langle dc||ji\rangle}{-(\varepsilon_c + \varepsilon_d - \varepsilon_i - \varepsilon_j)}, \end{aligned} \quad (34)$$

which turn out to be independent of the frequency. To the best of our knowledge, the matrix elements in Eq. (34) had never been given in the literature before. It is easy to check that the ov/vv block is Hermitian, $f_{c,\text{BSE2},ia,jb}(\omega) = f_{c,\text{BSE2},jb,ia}(\omega)^*$, and that the ov/vv block is symmetric, $f_{c,\text{BSE2},ia,bj} = f_{c,\text{BSE2},jb,ai}$.

The matrix elements of the BSE2 correlation kernel display sums over either one occupied and one virtual orbital (for the ph/hp terms) or over two occupied or two virtual orbitals (for the pp/hh terms). In a straightforward implementation, the computational cost of the latter scales as $N_o^2 N_v^4$ where N_o is the number of occupied orbitals and N_v the number of virtual ones. However, in the case of the long-range interaction, the computational cost of the BSE2 correlation kernel could be made low by approximating the long-range two-electron integrals by multipole expansions [34].

IV. PRACTICAL RESOLUTION AND COMPUTATIONAL DETAILS

A. Perturbative resolution

In the range-separated scheme that we propose, we approximate the inverse of the linear-response function as [combining Eqs. (1) and (7)]

$$\chi^{-1}(\omega) \approx \chi_0^{-1}(\omega) - f_{\text{Hxc},\text{HF}}^{\text{lr}} - f_{\text{Hxc}}^{\text{sr}} - f_{c,\text{BSE2}}^{\text{lr}}(\omega), \quad (35)$$

where $\chi_0(\omega)$ is the RSH non-interacting linear-response function and $f_{c,\text{BSE2}}^{\text{lr}}(\omega)$ is the BSE2 correlation kernel for the long-range electron-electron interaction. We note that, according to Eq. (23), instead of $\chi_0^{-1}(\omega)$, we should use in Eq. (35) the inverse of the long-range IP linear-response function $(\chi_{\text{IP}}^{\text{lr}})^{-1}(\omega)$ constructed with the long-range interacting Green function. This could be accounted for by either adding self-energy (or quasiparticle)

corrections to the orbital energies, as done in Ref. 18, or adding self-energy contributions to the long-range correlation kernel [20]. These contributions can generally be important when using HF orbitals or DFT orbitals with semilocal DFAs. However, in the case of range separation, the orbital energies obtained with long-range HF exchange are already good approximations to quasiparticle energies [35, 36]. It is thus reasonable to use the approximation $(\chi_{\text{IP}}^{\text{lr}})^{-1}(\omega) \approx \chi_0^{-1}(\omega)$.

When projected in the basis of the RSH spin-orbitals, Eq. (35) leads to the self-consistent pseudo-Hermitian eigenvalue equation

$$\begin{pmatrix} \mathbf{A}(\omega_n) & \mathbf{B} \\ \mathbf{B}^* & \mathbf{A}(-\omega_n)^* \end{pmatrix} \begin{pmatrix} \mathbf{X}_n \\ \mathbf{Y}_n \end{pmatrix} = \omega_n \begin{pmatrix} \mathbf{1} & \mathbf{0} \\ \mathbf{0} & -\mathbf{1} \end{pmatrix} \begin{pmatrix} \mathbf{X}_n \\ \mathbf{Y}_n \end{pmatrix}, \quad (36)$$

where ω_n are the excitation (or diexcitation) energies, $(\mathbf{X}_n, \mathbf{Y}_n)$ are the associated linear-response eigenvectors, and the matrix elements of \mathbf{A} and \mathbf{B} are given by

$$\begin{aligned} A_{ia,jb}(\omega) = & (\varepsilon_a - \varepsilon_i)\delta_{ij}\delta_{ab} + \langle aj|w_{\text{ee}}|ib\rangle - \langle aj|w_{\text{ee}}^{\text{lr}}|bi\rangle \\ & + f_{\text{xc},ia,jb}^{\text{sr}} + f_{c,\text{BSE2},ia,jb}^{\text{lr}}(\omega), \end{aligned} \quad (37)$$

and

$$\begin{aligned} B_{ia,jb} = & \langle ab|w_{\text{ee}}|ij\rangle - \langle ab|w_{\text{ee}}^{\text{lr}}|ji\rangle \\ & + f_{\text{xc},ia,bj}^{\text{sr}} + f_{c,\text{BSE2},ia,bj}^{\text{lr}}, \end{aligned} \quad (38)$$

where ε_p are the RSH spin-orbital energies, $\langle pq|w_{\text{ee}}|rs\rangle$ and $\langle pq|w_{\text{ee}}^{\text{lr}}|rs\rangle$ are two-electron integrals in the RSH spin-orbital basis associated with the Coulomb interaction w_{ee} and the long-range interaction $w_{\text{ee}}^{\text{lr}}$, respectively, and $f_{\text{xc},pq,rs}^{\text{sr}}$ are the matrix elements of the short-range exchange-correlation kernel. The matrix elements of the long-range BSE2 correlation kernel $f_{c,\text{BSE2},pq,rs}^{\text{lr}}$ are given in Eqs. (33) and (34) using in these expressions long-range two-electron integrals $\langle pq||rs\rangle \rightarrow \langle pq|w_{\text{ee}}^{\text{lr}}|rs\rangle - \langle pq|w_{\text{ee}}^{\text{lr}}|sr\rangle$ and RSH spin-orbital energies ε_p .

The resolution of the self-consistent eigenvalue equation (36) is more complicated than in the standard case of a frequency-independent matrix \mathbf{A} . Following Zhang *et al.* [18], for a first exploration of the method, we work within the TDA (i.e. we set $\mathbf{B} = \mathbf{0}$) and use a non-self-consistent perturbative resolution. We thus decompose the matrix \mathbf{A} in Eq. (37) as the sum of the frequency-independent RSH contribution [10] and the long-range frequency-dependent BSE2 correlation kernel contribution

$$\mathbf{A}(\omega) = \mathbf{A}_{\text{RSH}} + \mathbf{f}_{c,\text{BSE2}}^{\text{lr}}(\omega). \quad (39)$$

The TDRSH linear-response equation is first solved in the TDA,

$$\mathbf{A}_{\text{RSH}}\mathbf{X}_{0,n} = \omega_{0,n}\mathbf{X}_{0,n}, \quad (40)$$

where $\omega_{0,n}$ and $\mathbf{X}_{0,n}$ are the corresponding excitation energies and linear-response eigenvectors, respectively. The

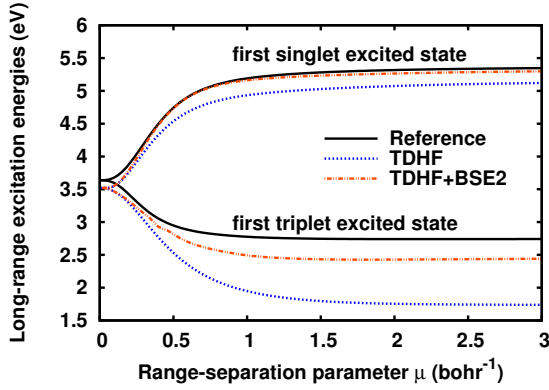


Figure 3: Long-range excitation energies to the first triplet and singlet excited states of the Be atom as a function of the range-separation parameter μ , obtained by long-range TDHF and long-range TDHF+BSE2 calculations in the TDA using RSH (with the short-range LDA functional) orbitals and an uncontracted d-aug-cc-pVDZ basis set. The reference FCI long-range excitation energies are from Ref. 39.

effect of the long-range BSE2 correlation kernel is then added perturbatively to obtain the excitation energies

$$\omega_n = \omega_{0,n} + Z_n \mathbf{X}_{0,n}^\dagger \mathbf{f}_{c,\text{BSE2}}^{\text{lr}}(\omega_{0,n}) \mathbf{X}_{0,n}, \quad (41)$$

where Z_n is the normalization factor

$$Z_n = \left(1 - \mathbf{X}_{0,n}^\dagger \left. \frac{\partial \mathbf{f}_{c,\text{BSE2}}^{\text{lr}}(\omega)}{\partial \omega} \right|_{\omega=\omega_{0,n}} \mathbf{X}_{0,n} \right)^{-1}. \quad (42)$$

As pointed out by Zhang *et al.* [18], the effect of the normalization factor Z_n turns out to be very small (Z_n is always very close to 1, especially in the range-separated case), but we keep it in our calculations. We note that the expression of the correction $\mathbf{X}_{0,n}^\dagger \mathbf{f}_{c,\text{BSE2}}^{\text{lr}}(\omega_{0,n}) \mathbf{X}_{0,n}$ in Eq. (41) is very similar (but not identical) to the so-called “direct” contribution of the CIS(D) correction [37, 38]. As for CIS(D), it is easy to check that $\mathbf{X}_{0,n}^\dagger \mathbf{f}_{c,\text{BSE2}}^{\text{lr}}(\omega_{0,n}) \mathbf{X}_{0,n}$ contains only connected terms and thus provides a size-consistent correction to the excitation energies.

The method defined by Eqs. (40) and (41) will be referred to as TDRSH+BSE2. For $\mu = 0$, all long-range contributions vanish, and it reduces to the standard time-dependent Kohn-Sham (TDKS) method in the TDA. For $\mu \rightarrow \infty$, all short-range contributions vanish, and it reduces to time-dependent Hartree-Fock (TDHF) within the TDA (i.e. CIS) with a BSE2 correction, which will be referred to as TDHF+BSE2.

B. Computational details

We calculate vertical excitation energies of four small molecules, N_2 , CO , H_2CO , and C_2H_4 , at their experimental geometries [40–43], using the Sadlej+ basis sets [44].

Our reference values are obtained by equation-of-motion coupled-cluster singles doubles (EOM-CCSD) calculations performed with GAUSSIAN 09 [45]. For each molecule, we report the first 14 excited states found with the EOM-CCSD method. For each molecule, we perform a self-consistent ground-state RSH calculation using the short-range LDA exchange-correlation functional of Ref. 46, followed by a spin-adapted closed-shell TDRSH linear-response calculation in the TDA using the short-range LDA exchange-correlation kernel [10], as implemented in a development version of MOLPRO [47]. The TDRSH+BSE2 excitation energies are then calculated by a spin-adapted closed-shell version of Eq. (41) implemented in a homemade software interfaced with MOLPRO (see Ref. 22 for details). The range-separation parameter μ is set to 0.35 bohr^{-1} which yields a minimal mean absolute deviation (MAD) over the four molecules of the TDRSH+BSE2 excitation energies with respect to the EOM-CCSD references. For comparison, we also perform standard, linear-response TDKS calculations with the LDA functional [48], as well as TDHF and TDHF+BSE2 calculations, all in the TDA. In the TDA, $X_{0,n,ia}$ can be considered as the coefficient of the (spin-orbital) single excitation $i \rightarrow a$ in the wave function of the excited state n . Each excited state was thus assigned by looking at its symmetry and at the leading orbital contributions to the excitation.

For the Be atom, we also perform calculations of long-range excitation energies as a function of μ , obtained by removing the contribution from the short-range Hxc kernel $f_{\text{Hxc}}^{\text{sr}}$ in the matrices $A_{ia,jb}$ and $B_{ia,jb}$ in Eqs. (37) and (38), i.e.

$$A_{ia,jb}^{\text{lr}}(\omega) = (\varepsilon_a - \varepsilon_i) \delta_{ij} \delta_{ab} + \langle aj | w_{\text{ee}}^{\text{lr}} | ib \rangle - \langle aj | w_{\text{ee}}^{\text{lr}} | bi \rangle + f_{c,\text{BSE2},ia,jb}^{\text{lr}}(\omega), \quad (43)$$

and

$$B_{ia,jb}^{\text{lr}} = \langle ab | w_{\text{ee}}^{\text{lr}} | ij \rangle - \langle ab | w_{\text{ee}}^{\text{lr}} | ji \rangle + f_{c,\text{BSE2},ia,bj}^{\text{lr}}, \quad (44)$$

using RSH orbitals and orbital energies (with the short-range LDA functional), and the TDA, as for the calculations on the molecules. The obtained long-range excitation energies are approximations to the excitation energies of the long-range interacting Hamiltonian of Eq. (2) and allow us to test the effect of the BSE2 correlation kernel independently of the approximation used for the short-range exchange-correlation kernel. For these calculations, we use an uncontracted d-aug-cc-pVDZ basis set for which we have reference long-range excitation energies obtained at the full configuration-interaction (FCI) level using an accurate Lieb-optimized short-range potential [39].

Table I: Excitation energies of N_2 calculated by linear-response TDKS (with the LDA functional), TDRSH and TDRSH+BSE2 (with the short-range LDA functional and $\mu = 0.35$ bohr $^{-1}$), TDHF and TDHF+BSE2, all within the TDA. The EOM-CCSD excitation energies are taken as reference. The Sadlej+ basis set is used.

State	Transition	TDKS	TDRSH	TDRSH+BSE2	TDHF	TDHF+BSE2	EOM-CCSD
Valence excitation energies (eV)							
$^3\Sigma_u^+$	$1\pi_u \rightarrow 1\pi_g$	8.08	7.74	7.93	6.23	8.88	7.72
$^3\Pi_g$	$3\sigma_g \rightarrow 1\pi_g$	7.58	7.85	8.05	7.99	10.97	8.16
$^3\Delta_u$	$1\pi_u \rightarrow 1\pi_g$	8.88	8.54	8.74	7.32	9.96	9.07
$^1\Pi_g$	$3\sigma_g \rightarrow 1\pi_g$	9.17	9.50	9.68	10.02	12.43	9.55
$^3\Sigma_u^-$	$1\pi_u \rightarrow 1\pi_g$	9.65	9.34	9.53	8.50	10.77	10.00
$^1\Sigma_u^-$	$1\pi_u \rightarrow 1\pi_g$	9.65	9.34	9.53	8.50	10.84	10.24
$^1\Delta_u$	$1\pi_u \rightarrow 1\pi_g$	10.25	9.98	10.18	9.06	11.30	10.66
$^3\Pi_u$	$2\sigma_u \rightarrow 1\pi_g$	10.42	10.77	10.97	11.74	14.82	11.36
Rydberg excitation energies (eV)							
$^3\Sigma_g^+$	$3\sigma_g \rightarrow 4\sigma_g$	10.28	11.47	11.56	13.12	13.94	11.74
$^1\Sigma_g^+$	$3\sigma_g \rightarrow 4\sigma_g$	10.40	11.94	11.98	14.01	14.22	12.15
$^3\Sigma_u^+$	$3\sigma_g \rightarrow 3\sigma_u$	10.63	12.30	12.40	14.21	15.07	12.70
$^3\Pi_u$	$3\sigma_g \rightarrow 2\pi_u$	10.99	12.30	12.36	13.04	13.43	12.71
$^1\Pi_u$	$3\sigma_g \rightarrow 2\pi_u$	10.98	12.39	12.44	13.23	13.45	12.77
$^1\Sigma_u^+$	$3\sigma_g \rightarrow 3\sigma_u$	10.62	12.43	12.51	14.31	15.04	12.82
Ionization threshold: $-\epsilon_{\text{HOMO}}$ (eV)							
		6.30	14.94		16.74		
MAD of excitation energies with respect to EOM-CCSD (eV)							
Valence		0.48	0.47	0.35	1.14	1.65	-
Rydberg		1.83	0.34	0.27	1.17	1.71	-
Total		1.06	0.41	0.32	1.15	1.68	-
Maximum absolute deviation of excitation energies with respect to EOM-CCSD (eV)							
		2.19	0.90	0.71	1.86	3.47	-

Table II: Same as Table I for CO.

State	Transition	TDKS	TDRSH	TDRSH+BSE2	TDHF	TDHF+BSE2	EOM-CCSD
Valence excitation energies (eV)							
$^3\Pi$	$5a_1(\sigma) \rightarrow 2e_1(\pi^*)$	6.04	6.10	6.32	5.85	8.27	6.45
$^3\Sigma^+$	$1e_1(\pi) \rightarrow 2e_1(\pi^*)$	8.54	8.45	8.63	7.79	10.38	8.42
$^1\Pi$	$5a_1(\sigma) \rightarrow 2e_1(\pi^*)$	8.42	8.68	8.88	9.08	10.94	8.76
$^3\Delta$	$1e_1(\pi) \rightarrow 2e_1(\pi^*)$	9.20	9.13	9.31	8.74	11.19	9.39
$^3\Sigma^-$	$1e_1(\pi) \rightarrow 2e_1(\pi^*)$	9.84	9.80	9.98	9.73	11.76	9.97
$^1\Sigma^-$	$1e_1(\pi) \rightarrow 2e_1(\pi^*)$	9.84	9.80	9.98	9.73	11.82	10.19
$^1\Delta$	$1e_1(\pi) \rightarrow 2e_1(\pi^*)$	10.33	10.32	10.50	10.15	12.05	10.31
$^3\Pi$	$4a_1(\sigma) \rightarrow 2e_1(\pi^*)$	11.43	11.96	12.12	13.31	15.70	12.49
Rydberg excitation energies (eV)							
$^3\Sigma^+$	$5a_1(\sigma) \rightarrow 6a_1(\sigma)$	9.56	10.34	10.46	11.18	12.09	10.60
$^1\Sigma^+$	$5a_1(\sigma) \rightarrow 6a_1(\sigma)$	9.95	11.12	11.20	12.27	12.61	11.15
$^3\Sigma^+$	$5a_1(\sigma) \rightarrow 7a_1(\sigma)$	10.26	11.08	11.17	12.42	12.83	11.42
$^1\Sigma^+$	$5a_1(\sigma) \rightarrow 7a_1(\sigma)$	10.50	11.30	11.38	12.79	12.91	11.64
$^3\Pi$	$5a_1(\sigma) \rightarrow 3e_1(\pi)$	10.39	11.26	11.34	12.60	13.20	11.66
$^1\Pi$	$5a_1(\sigma) \rightarrow 3e_1(\pi)$	10.50	11.45	11.52	12.88	13.21	11.84
Ionization threshold: $-\epsilon_{\text{HOMO}}$ (eV)							
		9.12	13.49		15.11		
MAD of excitation energies with respect to the EOM-CCSD calculation (eV)							
Valence		0.33	0.23	0.16	0.49	2.02	-
Rydberg		1.19	0.29	0.22	0.97	1.42	-
Total		0.70	0.26	0.19	0.69	1.76	-
Maximum absolute deviation of excitation energies with respect to EOM-CCSD (eV)							
		1.34	0.53	0.36	1.16	3.22	-

V. RESULTS AND DISCUSSION

A. Long-range excitation energies of the Be atom

The long-range excitation energies to the first triplet and singlet excited states of the Be atom are plotted as a function of the range-separation parameter μ in Figure 3. The triplet and singlet excitation energies are degenerate at $\mu = 0$, where they reduce to the non-interacting Kohn-Sham excitation energies. When increasing μ , i.e. when adding the long-range interaction, this degeneracy

is lifted and the excitation energies quickly tend to the physical excitation energies in the limit $\mu \rightarrow \infty$.

The TDHF long-range excitation energies are accurate close to $\mu = 0$, but they deteriorate as μ is increased. For $\mu \gtrsim 1$, TDHF underestimates the triplet long-range excitation energy by about 1 eV and the singlet long-range excitation energy by about 0.25 eV, in comparison to the reference FCI long-range excitation energies. Adding the long-range BSE2 correlation kernel correctly increases the TDHF long-range excitation energies, leading to an accurate singlet excitation energies for all μ and reducing the error in the TDHF triplet excitation energy

Table III: Same as Table I for H₂CO.

State	Transition	TDKS	TDRSH	TDRSH+BSE2	TDHF	TDHF+BSE2	EOM-CCSD
Valence excitation energies (eV)							
³ A ₂	2b ₂ (n) → 2b ₁ (π*)	3.08	3.17	3.45	3.76	6.86	3.56
¹ A ₂	2b ₂ (n) → 2b ₁ (π*)	3.70	3.82	4.11	4.58	7.37	4.03
³ A ₁	1b ₁ (π) → 2b ₁ (π*)	6.35	6.08	6.39	4.96	8.30	6.06
³ B ₁	5a ₁ (σ) → 2b ₁ (π*)	7.77	8.09	8.40	8.60	12.28	8.54
Rydberg excitation energies (eV)							
³ B ₂	2b ₂ (n) → 6a ₁ (σ)	5.85	6.83	6.92	8.17	8.63	6.83
¹ B ₂	2b ₂ (n) → 6a ₁ (σ)	5.93	7.01	7.08	8.56	8.72	7.00
³ B ₂	2b ₂ (n) → 7a ₁ (σ)	6.96	7.69	7.81	9.04	9.85	7.73
³ A ₁	2b ₂ (n) → 3b ₂ (σ)	6.73	7.77	7.83	9.24	9.58	7.87
¹ B ₂	2b ₂ (n) → 7a ₁ (σ)	7.04	7.91	8.00	9.41	9.78	7.93
¹ A ₁	2b ₂ (n) → 3b ₂ (σ)	6.78	7.93	7.97	9.53	10.01	7.99
¹ A ₂	2b ₂ (n) → 3b ₁ (π)	7.55	8.32	8.39	10.04	10.26	8.45
³ A ₂	2b ₂ (n) → 3b ₁ (π)	7.58	8.31	8.38	9.93	11.07	8.47
³ B ₂	2b ₂ (n) → 8a ₁ (σ)	7.97	8.90	8.98	10.21	11.96	8.97
¹ B ₂	2b ₂ (n) → 8a ₁ (σ)	8.19	9.17	9.25	10.86	11.05	9.27
Ionization threshold: -ε _{HOMO} (eV)							
		6.30	10.33		12.04		
MAD of excitation energies with respect to the EOM-CCSD calculation (eV)							
Valence		0.47	0.27	0.17	0.48	3.15	-
Rydberg		0.99	0.07	0.06	1.45	2.04	-
Total		0.84	0.13	0.09	1.17	2.36	-
Maximum absolute deviation of excitation energies with respect to EOM-CCSD (eV)							
		1.21	0.45	0.33	1.59	3.74	-

Table IV: Same as Table I for C₂H₄.

State	Transition	TDKS	TDRSH	TDRSH+BSE2	TDHF	TDHF+BSE2	EOM-CCSD
Valence excitation energies (eV)							
³ B _{1u}	1b _{3u} (π) → 1b _{2g} (π*)	4.74	4.35	4.73	3.54	6.06	4.41
¹ B _{1u}	1b _{3u} (π) → 1b _{2g} (π*)	7.91	8.07	8.38	7.70	9.11	8.00
³ B _{1g}	1b _{3g} (σ) → 1b _{2g} (π*)	7.18	7.92	8.04	8.48	10.43	8.21
¹ B _{1g}	1b _{3g} (σ) → 1b _{2g} (π*)	7.48	8.04	8.24	9.23	10.81	8.58
Rydberg excitation energies (eV)							
³ B _{3u}	1b _{3u} (π) → 4a _{1g} (σ)	6.59	7.21	7.35	6.91	7.37	7.16
¹ B _{3u}	1b _{3u} (π) → 4a _{1g} (σ)	6.65	7.36	7.48	7.14	7.43	7.30
³ B _{1g}	1b _{3u} (π) → 2b _{2u} (σ)	6.98	7.42	7.78	7.66	8.10	7.91
³ B _{2g}	1b _{3u} (π) → 3b _{1u} (σ)	7.10	8.03	8.11	7.79	8.07	7.93
¹ B _{1g}	1b _{3u} (π) → 2b _{2u} (σ)	7.19	7.92	8.17	7.75	8.09	7.97
¹ B _{2g}	1b _{3u} (π) → 3b _{1u} (σ)	7.15	8.13	8.20	7.92	8.07	8.01
³ A _g	1b _{3u} (π) → 2b _{3u} (π)	8.03	8.46	8.60	8.02	8.64	8.48
¹ A _g	1b _{3u} (π) → 2b _{3u} (π)	8.30	8.87	8.99	8.61	8.88	8.78
³ B _{3u}	1b _{3u} (π) → 5a _{1g} (σ)	8.26	8.97	9.12	8.74	9.26	9.00
¹ B _{3u}	1b _{3u} (π) → 5a _{1g} (σ)	8.28	9.09	9.20	8.92	9.13	9.07
Ionization threshold: -ε _{HOMO} (eV)							
		6.89	10.45		10.23		
MAD of excitation energies with respect to the EOM-CCSD calculation (eV)							
Valence		0.64	0.24	0.30	0.52	1.80	-
Rydberg		0.71	0.10	0.17	0.21	0.14	-
Total		0.69	0.14	0.21	0.30	0.62	-
Maximum absolute deviation of excitation energies with respect to EOM-CCSD (eV)							
		1.10	0.54	0.38	0.87	2.23	-

by a factor of 3 for large μ . These results are thus encouraging and support the relevance of the TDHF+BSE2 approximation for the long-range response kernel.

B. Excitation energies of the N₂, CO₂, H₂CO, and C₂H₄ molecules

The excitation energies for each method and each molecule are given in Tables I-IV. Mean absolute deviations (MAD) and maximum absolute deviations with respect to the EOM-CCSD reference are also given for valence, Rydberg, and all excitation energies.

As already well known, TDKS with the LDA func-

tional gives very underestimated Rydberg excitation energies. TDRSH greatly improves the excitation energies for the Rydberg states and, to a lesser extent, for the valence states, resulting in total MADs of 0.41, 0.26, 0.13, and 0.14 eV for N₂, CO₂, H₂CO, and C₂H₄, respectively. TDRSH also offers a more accurate description of valence and Rydberg excitation energies than TDHF. For a more intensive discussion of the performance of TDRSH, see Ref. 10.

Both when starting from TDHF and TDRSH, the addition of the BSE2 correlation correction always leads to larger excitation energies. In the case of TDHF, the BSE2 correction increases the valence excitation energies by about 2 or 3 eV, leading to largely overestimated va-

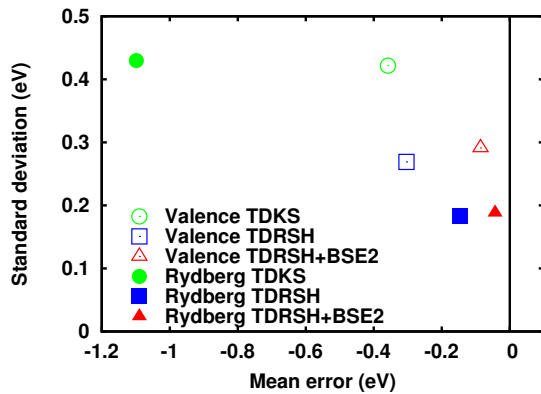


Figure 4: Mean error versus standard deviation for the valence and Rydberg excitation energies of the N_2 , CO_2 , H_2CO , and C_2H_4 molecules calculated with linear-response TDKS (with the LDA functional), TDRSH and TDRSH+BSE2 (with the short-range LDA functional and $\mu = 0.35$ bohr $^{-1}$), all within the TDA. The errors are calculated with respect to the EOM-CCSD excitation energies. The Sadlej+ basis set is used.

lence excitation energies. For Rydberg states, the BSE2 correction on top of TDHF is smaller (less than 1 eV) but also leads to systematically overestimated excitation energies. Overall, TDHF+BSE2 considerably worsens the TDHF excitation energies. We thus conclude that the relatively accurate results reported by Zhang *et al.* [18] crucially depend on using their *GW*-like second-order quasiparticle correction to the HF orbital energies, which we have not applied in this work.

In the range-separated case, the long-range BSE2 correction induces only a moderate increase of the valence excitation energies by about 0.2 to 0.4 eV, leading for these states to MADs of 0.35, 0.16, 0.17, and 0.30 eV for N_2 , CO_2 , H_2CO , and C_2H_4 , respectively. The TDRSH+BSE2 excitation energies of the Rydberg states are also systematically larger than the TDRSH ones by usually less than 0.1 eV, giving for these states MADs of 0.27, 0.22, 0.06, and 0.17 eV for N_2 , CO_2 , H_2CO , and C_2H_4 , respectively. Of course, the difference in magnitude of the BSE2 correction in the range-separated case compared to the full-range case is to be mostly attributed to the substitution of the full-range two-electron integrals by the long-range ones. Since for the chosen value of the range-separation parameter μ of 0.35 bohr $^{-1}$, TDRSH mostly gives slightly underestimated excitation energies of the considered systems, the long-range BSE2 correction overall slightly improves

the excitation energies. More specifically, in comparison with TDRSH, TDRSH+BSE2 gives slightly smaller total MADs of 0.32, 0.19, and 0.09 eV for N_2 , CO_2 , and H_2CO , and a slightly larger MAD of 0.21 eV for C_2H_4 . Also, for all the four molecules, TDRSH+BSE2 always gives the smallest maximum absolute deviation among all the methods, suggesting that TDRSH+BSE2 describes more reliably the excitation energies than the other methods.

Finally, as a global summary of the results, Figure 4 reports the mean error versus the standard deviation for the valence and Rydberg excitation energies of the four molecules for the different methods. For the valence excitation energies, going from TDKS to TDRSH mainly decreases the standard deviation, while going from TDRSH to TDRSH+BSE2 decreases the mean error. For the Rydberg excitation energies, TDRSH provides a large improvement over TDKS both in terms of mean error and standard deviation, while TDRSH+BSE2 gives a slightly smaller mean error than TDRSH.

VI. CONCLUSION

We have developed a range-separated linear-response TDDFT approach using a long-range frequency-dependent second-order Bethe-Salpeter correlation kernel. We have tested our approach using a perturbative resolution of the linear-response equations within the TDA for valence and Rydberg excitation energies of four small molecules. The results show that the addition of the long-range correlation kernel overall slightly improves the excitation energies.

More tests should now be carried out with this long-range correlation kernel to better assess its performance, in particular on systems having important effects from double excitations in their optical spectra. Also, a number of further developments should be explored: adding a self-energy (or quasiparticle) correction (either by doing a *GW*-like calculation or by including it in the correlation kernel), going beyond the TDA and the perturbative resolution of the linear-response equations, and going beyond the second-order approximation.

Acknowledgements

We thank J. A. Berger, E. Luppi, D. Mukherjee, L. Reining, P. Romaniello, and A. Savin for discussions.

-
- [1] E. K. U. Gross and W. Kohn, Phys. Rev. Lett. **55**, 2850 (1985).
 - [2] M. E. Casida, in *Recent Advances in Density Functional Methods, Part I*, edited by D. P. Chong (World Scientific, Singapore, 1995), p. 155.
 - [3] M. E. Casida, C. Jamorski, K. C. Casida, and D. R.

- Salahub, J. Chem. Phys. **108**, 4439 (1998).
- [4] A. Dreuw, J. L. Weisman, and M. Head-Gordon, J. Chem. Phys. **119**, 2943 (2003).
- [5] N. T. Maitra, F. Zhang, R. J. Cave, and K. Burke, J. Chem. Phys. **120**, 5932 (2004).
- [6] R. Bauernschmitt and R. Ahlrichs, Chem. Phys. Lett.

- 256**, 454 (1996).
- [7] Y. Tawada, T. Tsuneda, S. Yanagisawa, T. Yanai, and K. Hirao, *J. Chem. Phys.* **120**, 8425 (2004).
 - [8] T. Yanai, D. P. Tew, and N. C. Handy, *Chem. Phys. Lett.* **393**, 51 (2004).
 - [9] E. Livshits and R. Baer, *Phys. Chem. Chem. Phys.* **9**, 2932 (2007).
 - [10] E. Rebolini, A. Savin, and J. Toulouse, *Mol. Phys.* **111**, 1219 (2013).
 - [11] M. E. Casida, *J. Chem. Phys.* **122**, 054111 (2005).
 - [12] M. Huix-Rotllant and M. E. Casida, *Formal foundations of dressed time-dependent density-functional theory for many-electron excitations*, <http://arxiv.org/abs/1008.1478>.
 - [13] M. E. Casida and M. Huix-Rotllant, in *Density-Functional Methods for Excited States*, edited by N. Ferré, M. Filatov, and M. Huix-Rotllant (Springer, 2015), Topics in Current Chemistry.
 - [14] S. Grimme and F. Neese, *J. Chem. Phys.* **127**, 154116 (2007).
 - [15] K. Pernal, *J. Chem. Phys.* **136**, 184105 (2012).
 - [16] E. Fromager, S. Knecht, and H. J. A. Jensen, *J. Chem. Phys.* **138**, 084101 (2013).
 - [17] E. D. Hedegård, F. Heiden, S. Knecht, E. Fromager, and H. J. A. Jensen, *J. Chem. Phys.* **139**, 184308 (2013).
 - [18] D. Zhang, S. N. Steinmann, and W. Yang, *J. Chem. Phys.* **139**, 154109 (2013).
 - [19] S. Hirata and M. Head-Gordon, *Chem. Phys. Lett.* **314**, 291 (1999).
 - [20] D. Sangalli, P. Romaniello, G. Onida, and A. Marini, *J. Chem. Phys.* **134**, 034115 (2011).
 - [21] J. G. Ángyán, I. C. Gerber, A. Savin, and J. Toulouse, *Phys. Rev. A* **72**, 012510 (2005).
 - [22] E. Rebolini, PhD thesis, Université Pierre et Marie Curie (2014), URL <https://tel.archives-ouvertes.fr/tel-01027522>.
 - [23] E. Rebolini, J. Toulouse, and A. Savin, in *Electronic Structure and Reactivity*, edited by S. K. Ghosh and P. K. Chattaraj (CRC Press, 2013), Concepts and Methods in Modern Theoretical Chemistry Vol. 1, pp. 367–390, preprint at <http://arxiv.org/abs/1304.1314>.
 - [24] N. E. Dahlen and R. van Leeuwen, *Phys. Rev. Lett.* **98**, 153004 (2007).
 - [25] G. Baym and L. P. Kadanoff, *Phys. Rev.* **124**, 287 (1961).
 - [26] G. Baym, *Phys. Rev.* **127**, 1391 (1962).
 - [27] G. Strinati, *Rivista del Nuovo Cimento* **11**, 1 (1988).
 - [28] G. Csanak, H. Taylor, and R. Yaris (Academic Press, 1971), vol. 7 of *Adv. At. Mol. Phys.*, p. 287.
 - [29] P. Romaniello, D. Sangalli, J. A. Berger, F. Sottile, L. G. Molinari, L. Reining, and G. Onida, *J. Chem. Phys.* **130**, 044108 (2009).
 - [30] The last two terms of the kernel in Eq. (31) of Ref. 18 contain non-antisymmetrized two-electron integrals. However, these terms can also be written with a factor of 1/2 and antisymmetrized two-electron integrals, leading to our Eq. (33).
 - [31] J. Oddershede and P. Jørgensen, *J. Chem. Phys.* **66**, 1541 (1977).
 - [32] E. S. Nielsen, P. Jørgensen, and J. Oddershede, *J. Chem. Phys.* **73**, 6238 (1980).
 - [33] M. Huix-Rotllant, PhD thesis, Université de Grenoble (2011).
 - [34] G. Hetzer, M. Schütz, H. Stoll, and H.-J. Werner, *J. Chem. Phys.* **113**, 9443 (2000).
 - [35] T. Tsuneda, J.-W. Song, S. Suzuki, and K. Hirao, *J. Chem. Phys.* **133**, 174101 (2010).
 - [36] L. Kronik, T. Stein, S. Refaely-Abramson, and R. Baer, *J. Chem. Theory Comput.* **8**, 1515 (2012).
 - [37] M. Head-Gordon, R. J. Rico, M. Oumi, and T. J. Lee, *Chem. Phys. Lett.* **219**, 21 (1994).
 - [38] Y. M. Rhee and M. Head-Gordon, *J. Phys. Chem. A* **111**, 5314 (2007).
 - [39] E. Rebolini, J. Toulouse, A. M. Teale, T. Helgaker, and A. Savin, *Journal of Chemical Physics* **141**, 044123 (2014).
 - [40] K.-P. P. Huber and G. Herzberg, *Molecular Spectra and Molecular Structure - IV. Constants of Diatomic Molecules* (Van Nostrand Reinhold, New York, 1979).
 - [41] A. Le Floch, *Mol. Phys.* **72**, 133 (1991).
 - [42] L. V. Gurvich, I. V. Veyts, and C. B. Alcock, *Thermodynamic Properties of Individual Substances, Fourth Edition* (Hemisphere Pub. Co., New York, 1989).
 - [43] G. Herzberg, *Molecular spectroscopy and molecular structure; Electronic spectra and electronic structure of polyatomic molecules, vol. III* (van Nostrand Reinhold, New York, 1966).
 - [44] M. E. Casida, C. Jamorski, K. C. Casida, and D. R. Salahub, *J. Chem. Phys.* **108**, 4439 (1998).
 - [45] M. J. Frisch, G. W. Trucks, H. B. Schlegel, G. E. Scuseria, M. A. Robb, J. R. Cheeseman, G. Scalmani, V. Barone, B. Mennucci, G. A. Petersson, et al., *Gaussian 09 Revision A.1*, Gaussian Inc. Wallingford CT 2009.
 - [46] S. Pazziani, S. Moroni, P. Gori-Giorgi, and G. B. Bachelet, *Phys. Rev. B* **73**, 155111 (2006).
 - [47] H.-J. Werner, P. J. Knowles, G. Knizia, F. R. Manby, M. Schütz, and others, *Molpro, version 2012.1, a package of ab initio programs*, cardiff, UK, 2012, see <http://www.molpro.net>.
 - [48] J. P. Perdew and Y. Wang, *Phys. Rev. B* **45**, 13244 (1992).